HHS Public Access

Author manuscript

Antiviral Res. Author manuscript; available in PMC 2021 April 20.

Published in final edited form as:

Antiviral Res. 2018 January ; 149: 78–88. doi:10.1016/j.antiviral.2017.09.003.

Raltegravir blocks the infectivity of red-fluorescent-protein (mCherry)-labeled HIV-1_{JR-FL} in the setting of post-exposure prophylaxis in NOD/SCID/Jak3$^{-/-}$ mice transplanted with human PBMCs

Hiromi Ogata-Aoki[a,b], **Nobuyo Higashi-Kuwata**[a,c], **Shin-ichiro Hattori**[c,d], **Hironori Hayashi**[a,c], **Matthew Danish**[a], **Manabu Aoki**[a,b,e], **Chiemi Shiotsu**[f], **Yumi Hashiguchi**[g,h], **Akinobu Hamada**[i], **Hisataka Kobayashi**[j], **Hironobu Ihn**[f], **Seiji Okada**[d], **Hiroaki Mitsuya**[a,b,c,*]

[a] Departments of Hematology and Infectious Diseases, Kumamoto University Graduate School of Biomedical Sciences, Japan

[b] Experimental Retrovirology Section, National Cancer Institute, National Institutes of Health, Bethesda, MD, USA

[c] Experimental Retrovirology Section, Department of Refractory Viral Infection, National Center for Global Health and Medicine Research Institute, Tokyo, Japan

[d] Division of Hematopoiesis, Center for AIDS Research, Kumamoto University, Kumamoto, Japan

[e] Department of Medical Technology, Kumamoto Health Science University, Kumamoto, Japan

[f] Department of Dermatology and Plastic Surgery, Faculty of Life Sciences, Kumamoto University, Kumamoto, Japan

[g] Department of Clinical and Pharmaceutical Sciences, Faculty of Pharmaceutical Sciences, Kumamoto University, Kumamoto, Japan

[h] Department of Pharmacy, Kumamoto University Hospital, Kumamoto, Japan

[i] Division of Molecular Pharmacology, National Cancer Center Research Institute, Tokyo, Japan

[j] Molecular Imaging Program, National Cancer Institute, National Institutes of Health, Bethesda, MD, USA

Abstract

Employing NOD/SCID/Jak3$^{-/-}$ mice transplanted with human PBMCs (hNOJ mice) and replication-competent, red-fluorescent-protein (mCherry; mC)-labeled HIV-1_{JR-FL} (HIV_{mC}), we examined whether early antiretroviral treatment blocked the establishment of HIV-1 infection. The

* Corresponding author. Experimental Retrovirology Section, Department of Refractory Viral Infection, National Center for Global Health and Medicine Research Institute, 1-21-1 Toyama Shinjuku-ku, Tokyo, 162-8655, Japan. hmitsuya@helix.nih.gov, hmitsuya@hosp.ncgm.go.jp (H. Mitsuya).

Conflict of interest

All authors declare no conflict of interest.

Appendix A. Supplementary data

Supplementary data related to this article can be found at https://doi.org/10.1016/j.antiviral.2017.09.003.

use of hNOJ mice and HIV_{mC} enabled us to visually locate infection foci and to examine the early dynamics of HIV_{mC} infection without using a large amount of antiretroviral unlike in non-human primate models. Although when raltegravir (RAL) administration was begun 1 day after intraperitoneal (*ip*) inoculation of HIV_{mC}, no plasma p24 or plasma HIV-1-RNA (pRNA) were detected in 10 of 12 hNOJ $\left(hNOJ_{mC}^{RAL+}\right)$ mice as assessed on the last day of the 14-day continuous twice-daily RAL administration, all 10 untreated $hNOJ_{mC}$ $\left(hNOJ_{mC}^{RAL-}\right)$ mice became positive for p24 and pRNA and had significantly swollen lymph nodes in peritoneal cavity and abundant $p24^+/mC^+/CD3^+/CD4^+$ T cells and $p24^+/mC^+/CD68^+$ monocytes/macrophages were identified in their omenta and mesenteric lymphoid tissues/lymph nodes upon necropsy of the mice on day 14. In 12 $hNOJ_{mC}^{RAL+}$ mice, no significantly swollen lymph nodes were seen compared to $hNOJ_{mC}^{RAL+}$ mice; however, in the omentum of the 2 $hNOJ_{mC}^{RAL-}$ mice that were positive for pRNA and *in site* RNA, $mC^+/p24^+/CD3^+/CD83^+$ cells were identified, suggesting that viral breakthrough occurred later in the observation period. The present data suggest that the use of hNOJ mouse model and HIV_{mC} may shed light on the study of early-phase dynamics of HIV-1 infection and cellular events in post-exposure/pre-exposure prophylaxis.

Keywords

mCherry-labeled HIV-1 (HIVmC); NOD/SCID/Jak3−/− (NOJ) mice *In vivo* imaging; Raltegravir administration Post-exposure prophylaxis HIV-1 breakthrough

1. Introduction

In the research area of HIV-1 infection and AIDS, the construction of humanized animal models through transplantation of human tissues or immunocompetent cells into severely immunocompromised mice has allowed the development of small human tissue/cell-reconstituted HIV-1 infection animal models (Van Duyne et al., 2009). In our previous study, we utilized humanized mice, non-obese diabetic (NOD)-SCID, interleukin 2 receptor gamma (IL-2Rgamma)-chain-knocked-out (NOG) mice, and established a human peripheral blood mononuclear cells (hPBMC)-transplanted R5 $HIV\text{-}1_{JR\text{-}FL}$-infected NOG mouse and showed that the NOG mouse system serves as a small-animal HIV-1 infection/AIDS model and that AK602, an experimental CCR5 inhibitor, blocked the infection and propagation of R5-HIV-1 in that mouse model (Nakata et al., 2005). In 2008, a group led by Okada subsequently developed human $CD34^+$ cells-transplanted, NOD/SCID/Janus kinase 3 (Jak3) knockout (NOJ) mice (Okada et al., 2008). In 2009, using a further refined NOJ mouse model, in which massive and systemic HIV-1 infection occurs, human $CD4^+/CD8^+$ cell ratios significantly decrease, and high levels of HIV-1 viremia are achieved (Hattori et al., 2009), we demonstrated that a novel HIV-1 reverse transcriptase inhibitor, 4′-ethynyl-2-fluoro-2′-deoxyadenosine or EFdA, exerts potent anti-HIV-1 activity (Hattori et al., 2009; Nakata et al., 2007).

Various rodent models for HIV-1 infection and its treatment have been reported; however, determination and evaluation of the presence of HIV-1 in a variety of tissues and organs in such small animals are time-consuming and labor-intensive since the sites of HIV-1

replication are difficult to determine, thus enforcing to sacrifice all animals and to examine all the tissues and organs following the sacrifice (Denton et al., 2010; Nischang et al., 2012; Sun et al., 2007). In this regard, various molecular imaging techniques, including single photon emission computed tomography, magnetic resonance imaging, and optical imaging have been developed to promote the understanding of fundamental cellular and molecular events in organisms and small animals in a noninvasive manner for various research fields (Alford et al., 2009; Lee et al., 2016a, 2016b).

We have most recently reported the establishment of an animal model enabling us to examine the dynamics of HIV-1 infection and cellular events in the initial phases of HIV-1 infection using HIV_{mC} with hNOJ mice and the spectral fluorescence *in vivo* image capturing system, Maestro™ and MVX10-Nuance (Higashi-Kuwata et al., 2017). In the present study, using HIV_{mC}, hNOJ mice, and the fluorescence image capturing system, we attempted to examine whether an HIV-1 integrase inhibitor, raltegravir (RAL), effectively blocked the establishment of HIV_{mC} infection in the setting of post-exposure prophylaxis.

2. Materials and methods

2.1. Determination of RAL concentrations in plasma in hNOJ mice

For the determination of RAL (a gift from MSD K.K., Tokyo, Japan) concentrations in hNOJ mouse plasma samples using HPLC (model LC-6A; Shimadzu, Kyoto, Japan) (Hashiguchi et al., 2013), the conditions of RAL standardization were first established. More details are described in Supplemental Material.

2.2. Generation of a recombinant HIV-1 clone containing traceable fluorescence protein, mC fluorescent protein

In the generation of a full-length molecular infectious HIV-1 clone containing mC fluorescent protein, the PCR-mediated recombination method was used as previously described (Fang et al., 1999). We refer to this infectious recombinant HIV-1 as HIV_{mC} (Fig. 1A). More details are shown in Supplemental Material.

2.3. Transplantation of hPBMC into NOJ mice

The NOD-SCID-$Jak3^{-/-}$ (NOJ) mice used in the present study were 16–20 weeks old at the time of transplantation of hPBMC isolated from an HIV-1-seronegative donor. The hNOJ mice were generated by methods previously described (Hattori et al., 2009; Okada et al., 2008). More details are described in Supplemental Material.

2.4. Inoculation of HIV_{mC} into hNOJ mice

The transfection-derived virions (HIV_{mC}; 300 ng p24) were intraperitoneally inoculated into each mouse in 10 days after hPBMC transplantation. On day 14 after HIV_{mC} inoculation, we performed *in vivo* imaging, immunohistological staining, flow cytometry and measurement of plasma p24 and plasma HIV-1 RNA copies levels.

2.5. In vivo imaging of HIV_{mC} infection in hNOJ mice

The spectral fluorescence images were captured using Maestro™ *in vivo* imaging system (PerkinElmer), eliminating auto-fluorescence and providing multicolor flexibility and accuracy for both visible and near-infrared labels using multispectral acquisition and analysis. More details are described in Supplemental Material.

2.6. The detection of HIV-1 in the plasma

A fully automated chemiluminescent enzyme immunoassay system (Lumipulse F; Fujirebio, Inc., Tokyo, Japan) was employed for determination of the amounts of p24 antigen in murine plasma, of which titer ranges were from 50 to 5000 pg/ml as previously described (Koh et al., 2003; Nakata et al., 2005). The AMPLICOR HIV-1 monitor test kit, version 1.5 (Roche Diagnostics, Branchburg, N.J.) was used for plasma viral load quantification of which titer ranges were from <400 copies/ml to >750,000 copies/ml.

2.7. Immunohistochemical staining

Immunohistological staining was performed using a Histofine® MOUSESTAIN KIT (Nichirei) according to the manufacturer's instructions. More details are described in Supplemental Material.

2.8. Quantitative examination of lymph nodes

The locations of lymph nodes observed were visually confirmed. To determine the location and anatomical terminology of lymph nodes, we referred to "Patterns of lymphatic drainage in the adult laboratory rat" published by Tilney (1971). In the quantitative examination of lymph nodes in $hNOJ_{unexposed}$, $hNOJ_{mC}^{RAL+}$ and $hNOJ_{mC}^{RAL-}$ mice, the largest lymph node excised from each mouse was individually weighed and compared after removing surrounding tissues.

2.9. In situ hybridization

HIV-RNA probes were designed based on HIV gag sequences 1381 to 1560 and 1741 to 1920 reported for detection of HIV-RNA in formalin-fixed and paraffin-embedded tissues (Nakajima et al., 2003) and applied according to the QuantiGene ViewRNA assay protocol (Panomics/Affymetrix, Santa Clara, CA, USA) (Honkavuori et al., 2011).

More details are described in Supplemental Material.

2.10. Statistical analyses

Nonparametric statistical analyses were performed by using the Mann-Whitney *U* test (Statview, version 5.0; Abacus Concepts) and Bonferroni method (Stat Flex, 5.0 software; Artec). Assessment of correlations was carried out using the Fisher Exact test (JMP® software; SAS Institute). *P* values of <0.05 were defined as significant.

3. Results

3.1. Pharmacokinetics of RAL in BALB/c mice

In a previous PK study conducted by Massud et al. (2015), an oral dose of 50 mg/kg administered to monkeys achieved an average Cmax being 299 (129–924) ng/ml. Since oral bioavailability of a number of compounds varies among species, we chose to administer RAL intraperitoneally so that possible differences in the oral bioavailability would not affect the PK of RAL in the present study. When a dose of 20 mg/kg RAL was administered to mice twice daily, and plasma samples were collected 3 min to 24 h after the administration and subjected to high-performance liquid chromatography analysis, RAL concentrations reached the maximal level of 9.28 (19.3 μM) ± 1.04 μg/ml 15 min after the administration and the concentration subsequently declined rapidly (Fig. 1C).

Oral administration of 400 mg RAL produces a peak concentration of 1.63 μg/ml (3.38 μM) in humans (n = 20) (Rizk et al., 2012). Thus, the Cmax achieved in the mice in the present study (9.28 ± 1.04 μg/ml) was about 6-fold greater than the Cmax achieved in humans.

3.2. Human immune cells are widely populated in the mesenteric region of hNOJ$_{mC}$ mice

In order to elucidate early-phase dynamics of HIV-1 infection, we previously established the HIV$_{mC}$-infected hNOJ mouse model using replication-competent HIV$_{mC}$ and hNOJ mice, in which following intraperitoneal HIV$_{mC}$ inoculation, the mC signal was readily detected in the organs in the peritoneal cavity, making it possible to easily locate HIV$_{mC}$ infection foci, although lymph nodes were hardly identified in mice exposed to unlabeled HIV-1 (Higashi-Kuwata et al., 2017).

In the present study, we examined the cellular constituents in the mesenteric region of the peritoneal cavity of HIV$_{mC}$-unexposed hNOJ mice (hNOJ$_{unexposed}$ mice), hNOJ mice exposed to HIV$_{mC}$ and untreated with RAL (hNOJ$_{mC}^{RAL-}$ mice), and hNOJ mice exposed to HIV$_{mC}$ and treated with RAL (hNOJ$_{mC}^{RAL+}$ mice). In line with our previous findings (Higashi-Kuwata et al., 2017), cells positive for hCD45 antigen (pan-human leucocyte marker) were found to be diffusely populated in the greater omentum (referred to as the omentum) and mesenteric lymph nodes in all hNOJ$_{unexposed}$, hNOJ$_{mC}^{RAL-}$, and hNOJ$_{mC}^{RAL+}$ mice (Fig. 1–D).

We further examined the profiles of human cell re-population in the three mouse groups. Morphologically, no apparent germinal centers or follicular structures were seen in all the mice examined. Fig. 2–A shows immunohistochemical staining results of the lymphoid tissues from each mouse group. In hNOJ$_{unexposed}$ mice, no mC$^+$ or p24$^+$ cells were seen, while the tissues contained substantial numbers of hCD45$^+$, hCD68$^+$, hCD3$^+$, hCD4$^+$ and hCD8$^+$ cells. In hNOJ$_{mC}^{RAL-}$ mice examined (n = 6), mC$^+$ and p24$^+$ cells were abundantly seen, together with hCD45$^+$, hCD68$^+$, hCD3$^+$, hCD4$^+$, and hCD8$^+$ cells. By contrast, no mC$^+$ or p24$^+$ cells were seen in hNOJ$_{mC}^{RAL+}$ mice examined (n = 6), while the numbers of hCD45$^+$, hCD68$^+$, hCD3$^+$, hCD4$^+$, and hCD8$^+$ cells were roughly comparable to those in hNOJ$_{mC}^{RAL-}$ mice (Fig. 2–A and –B). It was noted that hCD20$^+$ cells were not identified in lymphoid tissues from the hNOJ$_{unexposed}$ mice (n = 6), while significant numbers of hCD20$^+$

cells were seen in all the $hNOJ_{mC}^{RAL-}$ and $hNOJ_{mC}^{RAL+}$ mice (Fig. 2–A and –B), suggesting that the inoculum containing HIV_{mC} stimulated otherwise scarce and unidentifiable $hCD20^+$ cells and those cells proliferated to become visually identified regardless of HIV_{mC} exposure.

3.3. Effects of RAL on HIV_{mC} replication in hNOJ mice

The effects of RAL on HIV_{mC} replication was examined in hNOJ mice exposed to HIV_{mC}. NOJ mice irradiated with 1 Gy X-ray were intraperitoneally transplanted with hPBMC (2×10^7 cells/mouse) and were inoculated with HIV_{mC} 10 days after transplantation. Twenty-four hours later, RAL (20 mg/kg) was intraperitoneally administered twice a day for 14 days (Fig. 1–B) and PBMC and plasma samples were collected from murine peripheral blood on day 14 after the HIV_{mC} inoculation. HIV-1 plasma p24 antigen levels and HIV RNA copy number were determined in hNOJ mice exposed to HIV_{mC} and treated with RAL ($hNOJ_{mC}^{RAL+}$ mice) and hNOJ mice exposed to HIV_{mC} but not treated with RAL ($hNOJ_{mC}^{RAL-}$ mice). The amount of HIV-1 p24 in plasma proved to be high in $hNOJ_{mC}^{RAL-}$ mice, ranging from 4.4×10^2 to 2.5×10^5 pg/ml (5.5×10^3 pg/ml) (Fig. 3A), while no p24 antigen was found in plasma samples from $hNOJ_{mC}^{RAL+}$ mice as examined on day 14, suggesting that RAL blocked the replication and p24 production of HIV_{mC} ($P = 0.0003$) (Fig. 3–A).

As determined on day 14, HIV-1 RNA copy numbers in plasma samples were also high in $hNOJ_{mC}^{RAL-}$ mice, ranging from 8.0×10^4 to 2.7×10^7 copies/ml (3.3×10^6 copies/ml) (Fig. 3–B). However, plasma samples from 10 of 12 $hNOJ_{mC}^{RAL+}$ mice contained no HIV-1 RNA copies, while those from 2 of 12 $hNOJ_{mC}^{RAL+}$ mice contained significant levels of HIV-1 RNA copies (8.9×10^4 and 2.0×10^5 copies/ml) (Fig. 3–B). These data suggest that the RAL administration was mostly capable of blocking HIV_{mC} replication over the present 14-day observation period.

We also determined the numbers of $hCD4^+$ T cells in peripheral blood of the three mouse groups with flow cytometry using anti-mCD45, anti-hCD45, anti-hCD3, and anti-hCD4 on day 14. There was a significant decrease in the number of $hCD4^+$ T cells in the $hNOJ_{mC}^{RAL-}$ and $hNOJ_{mC}^{RAL+}$ mouse groups as compared to that in the $hNOJ_{unexposed}$ mouse group ($P < 0.006$ and $0.01 < P < 0.05$, respectively), while there was no significant difference in the $hCD4^+$ T cell numbers between the $hNOJ_{mC}^{RAL-}$ and $hNOJ_{mC}^{RAL+}$ mouse groups (Fig. 3–C). The reason why the $hCD4^+$ T cell numbers were not significantly different between the $hNOJ_{mC}^{RAL-}$ and $hNOJ_{mC}^{RAL+}$ mouse groups, is not clear (Fig. 3–C).

3.4. Visualization of HIV_{mC} infection in hNOJ mice and alteration of visualization under the treatment of RAL

We then attempted to examine the nature of mC signal-positive cells seen in the organs in $hNOJ_{mC}^{RAL-}$ and $hNOJ_{mC}^{RAL+}$ mice. In the present study, we examined how RAL administration impacted the early dynamics of HIV_{mC} infection in HIV_{mC}-exposed hNOJ mice. As shown

in Fig. 4–A-a and –d, when $hNOJ_{mC}^{RAL-}$ mice (n = 10) were sacrificed and mC-positive organs were excised out on day 14 following the HIV_{mC} inoculation, the mC signal was readily located in the serous membrane of the omentum and mesenteric lymph nodes using Maestro™. As expected, in the 10 $hNOJ_{mC}^{RAL+}$ mice, in which no p24 antigens or pRNA copies were detected in their plasma samples, no mC signal was identified (Fig. 4–A-b and –e). However, in the 2 $hNOJ_{mC}^{RAL+}$ mice, in which no p24 antigens were detected but ~10^5 pRNA copies/ml were found, only dim mC signals were seen while no distinct or condensed mC-positive lymph nodes were observed (Fig. 4A–c and f), indicating that the RAL dose employed failed to block the initial establishment of HIV_{mC} in the omentum, permitting the breakthrough of HIV_{mC} infection in the 2 $hNOJ_{mC}^{RAL+}$ mice. The $hNOJ_{mC}^{RAL+}$ mice that were positive for pRNA are referred as $hNOJ_{mC}^{RAL+/pRNA+}$ mice, while $hNOJ_{mC}^{RAL+}$ mice that were negative for pRNA as $hNOJ_{mC}^{RAL+/pRNA-}$ mice. As examined on day 14, a number of $p24^+$ cells were seen in the omentum and mesenteric lymph nodes in all $hNOJ_{mC}^{RAL-}$ mice. However, no $p24^+$ cells were detected in the 10 $hNOJ_{mC}^{RAL+/pRNA-}$ mice, while in the 2 $hNOJ_{mC}^{RAL+/pRNA+}$ mice, a substantial number of $p24^+$ cells were seen in the omentum (Fig. 4–B).

In order to confirm that the positivity of mC signal reflects the establishment of HIV_{mC} infection and its expression, we further conducted immunohistochemical double-staining of the omentum tissues from four mouse groups (n = 2 to 6). Fig. 4–C shows representative immunohistochemical profiles. In $hNOJ_{unexposed}$ mice, no mC or p24 signals were seen, although substantial numbers of human cells positive for hCD3 were identified (Fig. 4–C, top panel). However, in $hNOJ_{mC}^{RAL-}$ mice, mC^+ cells were abundantly identified in $hCD3^+$ cells. Those mC^+, $hCD3^+$ cells were also positive for p24. When *in situ* RNA hybridization was conducted in order to confirm the HIV-l-specificity, a number of HIV-1-RNA^+ cells were seen in the omentum tissues from $hNOJ_{mC}^{RAL-}$ mice. As expected, no mC or p24 signals were seen in the tissues from $hNOJ_{mC}^{RAL+/pRNA-}$ mice. This finding was further confirmed by the negativity in *in situ* hybridization. However, in $hNOJ_{mC}^{RAL+/pRNA+}$ mice, a significant number of mC^+, $p24^+$ cells were seen in $hCD3^+$ and $hCD83^+$ cells although such cells were scarce as compared to those in $hNOJ_{mC}^{RAL-}$ mice. The positivity for mC and p24 was also confirmed by *in situ* hybridization (Fig. 4–C, bottom panel) in the omentum tissues from $hNOJ_{mC}^{RAL+/pRNA+}$.

3.5. $hNOJ_{mC}^{RAL-}$ mice have a higher number and greater sizes of mesenteric lymph nodes than $hNOJ_{mC}^{RAL+}$ mice

In the previous study (Higashi-Kuwata et al., 2017), we reported that the enlarged mesenteric lymph nodes were identified in HIV_{mC}-exposed hNOJ mice. In general, the mesenteric lymph nodes are small and cannot be easily located with the naked eye in hNOJ mice as well as other humanized immunodeficiency mice, and even following HIV-1

infection, mesenteric lymph nodes are hardly identified. However, the use of HIV_{mC} made it possible to easily locate such lymph nodes. Our previous data showed that the number and weight of mesenteric lymph nodes are significantly greater in HIV_{mC}-exposed hNOJ mice than in unexposed hNOJ mice (Higashi-Kuwata et al., 2017). Therefore, in the present study, we attempted to determine the number and weight of mesenteric lymph nodes in $hNOJ_{mC}^{RAL-}$ and $hNOJ_{mC}^{RAL+}$ mice, both of which had been exposed to HIV_{mC}. Each of the mesenteric lymph nodes visually located and dissected was carefully stripped of surrounding tissues and the wet weight was measured using microbalance. Fig. 5–A shows all the weights of the mesenteric lymph nodes of the greatest size in each mouse. We failed to locate and identify mesenteric lymph nodes in $hNOJ_{unexposed}$ mice since they were of such small sizes and had no signals. Thus, those weights in 10 hNOJ mice are expressed as “zero” mg in Fig. 5–A. However, in $hNOJ_{mC}^{RAL-}$ mice, a number of mesenteric lymph nodes were readily located with significant and condensed signals (using Maestro™), solidly palpated, and effortlessly dissected from their surrounding tissues. As shown in Fig. 5–A, nine of the ten $hNOJ_{mC}^{RAL-}$ mice had swollen mesenteric lymph nodes of the weights ranging from ~0.01 to 0.6 mg. By contrast, no mC signals were seen in the abdominal cavity of all the twelve $hNOJ_{mC}^{RAL+}$ mice and we barely identified and dissected one likely mesenteric lymph node in three $hNOJ_{mC}^{RAL+}$ mice. It was possible, however, that each of these three lymph nodes represented a solitary lymph node such as a gut-associated lymphoid nodule (Kuper, 2006) and is not HIV-1-infection-associated swollen lymph node. In this regard, it should be noted that in the 2 $hNOJ_{mC}^{RAL+/pRNA+}$ mice, no swollen lymph nodes were seen as highlighted in blue in Fig. 5–A. We also determined the numbers of lymph nodes in all the mice. All six $hNOJ_{unexposed}$ mice had no identifiable lymph nodes, while all ten $hNOJ_{mC}^{RAL-}$ mice had significant numbers of readily identifiable mC-signal-emitting mesenteric lymph nodes. However, none of twelve $hNOJ_{mC}^{RAL+}$ mice had no identifiable mC-signal-emitting lymph nodes, although two of the twelve mice had one likely lymph node (Fig. 5–B). The observation that no mC signals were seen in the peritoneal cavity of all the $hNOJ_{mC}$ mice suggests that RAL administration in the present study may have blocked the infection and/or propagation in the HIV_{mC}-exposed mice as assessed over the 14-day period of treatment. However, to conclude that RAL treatment blocked HIV_{mC}, infection, no viral rebound following the cessation of the treatment should be confirmed.

3.6. No multinuclear giant cells or cytolysis were seen in successfully RAL-treated $hNOJ_{mC}$ mice

Since RAL treatment blocked the infection of HIV_{mC} in 10 of 12 $hNOJ_{mC}$ mice but 2 such mice underwent HIV_{mC} breakthrough as described above, we immunohistologically examined the lymphoid tissues/lymph nodes in the mesenteric region of all the mice. In the lymphoid tissues of $hNOJ_{unexposed}$, multi-nuclear giant cells or cytolysis, a salient feature of HIV-1 infection (Dargent et al., 2000), were not identified and all human lymphocytes and human monocytes/macrophages (shown by arrows in Fig. 6–A) appeared morphologically normal. However, in the mesenteric lymph nodes of $hNOJ_{mC}^{RAL-}$ mice, a number of mC^{+}

multi-nuclear cells (shown by arrows in Fig. 6–B) were readily identified with cytolytic feature. No multi-nuclear cells were identified in the lymphoid tissues from either of $hNOJ_{mC}^{RAL+/pRNA-}$ (Fig. 6–C) or $hNOJ_{mC}^{RAL+/pRNA+}$ mice. However, apparent lytic feature of mC^+ cells was observed (Fig. 6–D) in the lymphoid tissues of one of the two $hNOJ_{mC}^{RAL+/pRNA+}$ mice. The observation that abnormal morphology was identified in only one of the two $hNOJ_{mC}^{RAL+/pRNA+}$ mice suggest that the two $hNOJ_{mC}^{RAL+/pRNA+}$ mice probably had just undergone HIV_{mC} breakthrough.

4. Discussion

In the present work, employing hNOJ mice, HIV_{mC}, and an *in vivo* fluorescence image capturing system, we examined whether early antiretroviral treatment using an HIV-1 integrase inhibitor, RAL, blocked the productive HIV-1 infection. The reason why RAL was chosen as an antiretroviral agent in the present study is three-fold: (i) unlike protease inhibitors, RAL does not require a booster; (ii) a once-daily dose of RAL has been approved in May 2017 and could be used more widely; and (iii) RAL (in a long-acting formulation) has been shown to potently block HIV-infection in humanized BLT mice (Kovarova et al., 2016).

As shown in Fig. 1–D and 5, we demonstrated that even following transplantation of hPBMC to hNOJ mice, lymph nodes remained shrunk and appeared remnant and were hardly identified in $hNOJ_{unexposed}$ and $hNOJ_{mC}^{RAL+}$ mice. However, in $hNOJ_{mC}^{RAL-}$ mice, with the use of HIV_{mC} combined with the *in vivo* imaging system using Maestro™, lymph nodes were readily identified and we subjected those to various examinations. Of note, those lymph nodes were visibly swollen compared to $hNOJ_{unexposed}$ mice, no germinal centers or follicular structures were observed. In line with our previous observation (Higashi-Kuwata et al., 2017), human lymphocytes and monocytes/macrophages were well distributed in various lymphoid tissues in all hNOJ mice (Fig. 2). In hNOJ mice infected with HIV_{mC} but untreated ($hNOJ_{mC}^{RAL-}$ mice), as expected, an increased number of mC^+ and $p24^+$ cells were seen (Fig. 2–B), although no changes in $hCD68^+$, $hCD3^+$, $hCD4^+$, or $hCD8^+$ cells were seen. However, in both $hNOJ_{mC}^{RAL-}$ and $hNOJ_{mC}^{RAL+}$ mice, moderate increase of $hCD20^+$ cells were seen. Such increase of hCD20+ cells in both RAL-treated and -untreated mice suggested that the HIV_{mc} inoculum contained various allogeneic antigens within the cellular debris of human-derived 293T cells, in which HIV_{mC} was propagated, such antigens stimulated otherwise scarce and unidentifiable $hcD20^+$ cells, and those cells proliferated to become visually identified regardless of HIV_{mC} infection/replication. It is also possible that HIV_{mC} particles *per se* within the inoculum served as polyclonal B-cell stimulators (Yarchoan et al., 1986) and caused the proliferation of $hCD20^+$ cells without regard to the establishment of HIV_{mC} infection. The immunologic activation of human cells by human allogeneic antigens and/or HIV_{mC} particles is assumed to have taken place in antigen-presenting cells such as dendritic cells that upon activation migrate to lymphoid tissues, where they interact T- and B-cells and mediate immune responses. Harman's group has reported that the expression of the maturation marker CD83 is up-regulated in mature monocyte-derived dendritic cells

upon HIV-1 infection (Harman et al., 2006). As expected, $hCD83^+$ cells (representing human activated dendritic cells including HIV_{mC}-infected dendritic cells) proved to be positive for mC signals (Fig. 4–C).

In the present study, two of the 12 $hNOJ_{mC}^{RAL+}$ mice turned out to be positive for pRNA copies (~10^5/ml), although those two mice were negative for plasma p24 antigen and the numbers of RNA copies were significantly less than those in $hNOJ_{mC}^{RAL-}$ mice (Fig. 3). These two $hNOJ_{mC}^{RAL+/pRNA+}$ mice were confirmed to have undergone HIV_{mC} breakthrough as examined with immunohistochemical double-staining and *in situ* hybridizatioin (Fig. 4–C). However, the number of mC^+, $p24^+$, or *in situ* RNA^+ cells appeared to be less compared to those in $hNOJ_{mC}^{RAL-}$ mice, suggesting that these two mice just had viral breakthrough at the time of sacrifice. In this regard, we first suspected that the two $hNOJ_{mC}^{RAL+/pRNA+}$ mice had viral breakthrough since rather dim but significant mC signals were detected in the serous membrane of the omentum as examined using the Maestro™ technology (Fig. 4–A). It is also possible that the apparent lower $mC^+/p24^+$/*in situ* RNA^+ signals in the two $hNOJ_{mC}^{RAL+/pRNA+}$ mice than those in $hNOJ_{mC}^{RAL-}$ mice may reflect that the two mice were infected and the relatively low viral load was maintained by the RAL treatment and the blunting of the HIV replication ensued (Garcia-Lerma et al., 2008). We did not initially conduct HIV PCR assays when we sacrificed the mice and obtained the fresh tissues. Only after we generated the data set showing that no plasma p24 or plasma HIV-l-RNA (pRNA) were detected in 10 of 12 hNOJ ($hNOJ_{mC}^{RAL+}$) mice over the 14-day observation, we attempted to conduct PCR assays using paraffin-embedded tissues. However, for some unknown technical problems (e.g., poor DNA extraction and such), we could not reproducibly gain the PCR signal. These data suggest that as shown in a post-exposure prevention study using simian immunodeficiency virus by Tsai et al. (1998), due to the time between virus exposure and treatment initiation that is a crucial factor for prevention of infection, a part of $hNOJ_{mC}^{RAL+}$ had eventual viral breakthrough but other 10 $hNOJ_{mC}^{RAL+}$ mice had no breakthrough during the 14 day-period of observation in the present study. It is possible that the use of greater doses of RAL or the same dose of RAL combined with other antiretroviral agent(s) could have prevented the viral breakthrough seen in the two $hNOJ_{mC}^{RAL+/pRNA+}$ mice. It is also possible that more $hNOJ_{mC}^{RAL+}$ mice could have viral breakthrough if the observation period in the present study had been extended. Of note, the nature of the mCherry-encoding gene deletion and 2-week interval observation poses a limit in interpreting the absence of $mC^+/p24^+$/*in situ* RNA^+ signals in the present data as a successful prophylaxis. Moreover, a relatively long-term examination as to whether or not such $mC^+/p24^+$/*in situ* RNA^+ signals remains negative following RAL washout is required to assure that prophylaxis was successful. However, the present experimental design was only 14 days and no further observation was made after washout. One reason is that as shown in Fig. 1–E of our previous paper first describing the present mouse system (Higashi-Kuwata et al., 2017), the mCherry-encoding gene persisted within PBMCs obtained from the HIV_{JR-FL}^{mC}-infected hNOJ mice over 14 days following HIV_{JR-FL}^{mC} inoculation; however,

deletion of the mCherry-encoding gene apparently occurred by day 21 after the inoculation. Thus, we planned to conduct the 14-day interval examination in the present study.

When we determined the numbers of $hCD4^+$ T cells in peripheral blood of the three mouse groups on day 14, there was a significant decrease in the number of $hCD4^+$ T cells in the $hNOJ_{mC}^{RAL+}$ and $hNOJ_{mC}^{RAL-}$ mouse groups as compared to that in $hNOJj_{unexposed}$ ($P < 0.006$ and $0.01 < P < 0.05$, respectively) (Fig. 3–C). Since HIV_{mC} infection was efficiently blocked in $hNOJ_{mC}^{RAL+}$ mice (Fig. 3–A and –B), the reason why the $hCD4^+$ T cell numbers in the $hNOJ_{mC}^{RAL-}$ and $hNOJ_{mC}^{RAL+}$ mouse groups were significantly less compared to those in $hNOJ_{unexposed}$ mice is not readily understood. In this regard, it is possible that the R5 envelope glycoprotein of HIV_{mC}, which originated from R5-$HIV\text{-}1_{JR\text{-}FL}$ employed as a source of infectious virions in the present study, caused R5-induced apoptosis of $hCD4^+$ cells, resulting in the decrease of $hCD4^+$ cells in both $hNOJ_{mC}^{RAL+}$ mouse group (Wade et al., 2010). In terms of the possible down-regulation of CD4 antigen expression by NEF (Levesque et al., 2004), the virus HIV_{mC} expressed no NEF when assessed with western blot using the $pHIV_{mC}$-transfected COS-7 cell lysates and virion (HIV_{mC}) lysates, as we described in our previous paper authored by Higashi-Kuwata, Ogata-Aoki et al. (Higashi-Kuwata et al., 2017). The absence of NEF expression is probably due to the insertion of the mCherry-encoding gene in place of the NEF-encoding region in $HIV\text{-}1_{JR\text{-}FL}$. It is also possible that HIV-1 infection was established and subsequently viral replication was controlled by RAL treatment so that the $hNOJ_{mC}^{RAL+}$ mice became apparently negative for HIV-1 indices, leaving the significant reduction in $hCD4^+$ T cells in such mice. Such possibility cannot be excluded in the absence of early sampling and a more detailed analysis of HIV DNA in tissues. The numbers of $hCD4^+$ cells in Fig. 2–B were determined with thin sectioned mesenteric lymph node samples derived from 6 mice of $hNOJ_{unexposed}$, $hNOJ_{mC}^{RAL-}$, and $hNOJ_{mC}^{RAL+}$ groups using the highperformance image processing/analysis/measurement software WinROOF. No significant differences were found among the three samples. In contrast, the numbers of $hCD4^+$ cells in Fig. 3 were determined with peripheral blood mononuclear cells in 10 $hNOJ_{unexposed}$ mice, 8 $hNOJ_{mC}^{RAL-}$ mice and 12 $hNOJ_{mC}^{RAL+}$ mice using flow-cytometry. Thus, the apparent discrepancy between Figs. 2B and 3C may be due to the statistical power of the greater numbers of the samples in Fig. 3C. It is also possible that although $CD4^+$ cells in tissues are from only one site (one mesenteric lymph node only), which may not reflect the number of $CD4^+$ T-cell in the entire tissues/organs. The number of $CD4^+$ T-cells in peripheral blood perhaps does not deviate due to the sampling site. It is also possible that the discrepancy may reflect a compartmental variation in the three mice groups ($hNOJ_{unexposed}$, $hNOJ_{mC}^{RAL-}$, and $hNOJ_{mC}^{RAL+}$ mice).

The present study, taken together, strongly suggest that the use of the current hNOJ mouse model employing HIV_{mC} as a source of infectious virions is of utility and should shed light on the study of early-phase dynamics of HIV-1 transmission and cellular events as well as in the research area of pre-exposure and post-exposure prophylaxis of HIV-1 infection.

Supplementary Material

Refer to Web version on PubMed Central for supplementary material.

Acknowledgments

The authors thank Y. Yonemura, R. Kariya, and K. Maeda for valuable comments and suggestions. The present work was supported in part by a Grant for Development of Novel Drugs for Treating HIV-1 Infection and AIDS from japan Agency for Medical Research and Development (AMED) (H.M.), Grants from japan Society for the Promotion of Sciences (jSPS KAKENHI Grant Numbers jP16K15520 and jP26293239) (H.M.), a Grant from National Center for Global Health & Medicine (H.M.), and a Grant from the Intramural Research Program of Center for Cancer Research, National Cancer Institute, National Institutes of Health (H.K., H.M.).

References

Alford R, Ogawa M, Choyke PL, Kobayashi H, 2009. Molecular probes for the in vivo imaging of cancer. Mol. Biosyst. 5,1279–1291. [PubMed: 19823742]

Dargent JL, Lespagnard L, Kornreich A, Hermans P, Clumeck N, Verhest A, 2000. HIV-associated multinucleated giant cells in lymphoid tissue of the Waldeyer's ring: a detailed study. Mod. Pathol. 13,1293–1299. [PubMed: 11144925]

Denton PW, Krisko JF, Powell DA, Mathias M, Kwak YT, Martinez-Torres F, Zou W, Payne DA, Estes JD, Garcia JV, 2010. Systemic administration of antiretrovirals prior to exposure prevents rectal and intravenous HIV-1 transmission in humanized BLT mice. PLoS One 5, e8829. [PubMed: 20098623]

Fang G, Weiser B, Visosky A, Moran T, Burger H, 1999. PCR-mediated recombination: a general method applied to construct chimeric infectious molecular clones of plasma-derived HIV-1 RNA. Nat. Med. 5, 239–242. [PubMed: 9930876]

Garcia-Lerma JG, Otten RA, Qari SH, Jackson E, Cong ME, Masciotra S, Luo W, Kim C, Adams DR, Monsour M, Lipscomb J, johnson JA, Delinsky D, Schinazi RF, Janssen R, Folks TM, Heneine W, 2008. Prevention of rectal SHIV transmission in macaques by daily or intermittent prophylaxis with emtricitabine and tenofovir. PLoS Med. 5, e28. [PubMed: 18254653]

Harman AN, Wilkinson J, Bye CR, Bosnjak L, Stern JL, Nicholle M, Lai J, Cunningham AL, 2006. HIV induces maturation of monocyte-derived dendritic cells and Langerhans cells. J. Immunol. 177, 7103–7113. [PubMed: 17082627]

Hashiguchi Y, Hamada A, Shinohara T, Tsuchiya K, Jono H, Saito H, 2013. Role of P-glycoprotein in the efflux of raltegravir from human intestinal cells and CD4+ T-cells as an interaction target for anti-HIV agents. Biochem. Biophys. Res. Commun. 439, 221–22. [PubMed: 23981805]

Hattori S, Ide K, Nakata H, Harada H, Suzu S, Ashida N, Kohgo S, Hayakawa H, Mitsuya H, Okada S, 2009. Potent activity of a nucleoside reverse transcriptase inhibitor, 4′-ethynyl-2-fluoro-2′-deoxyadenosine, against human immunodeficiency virus type 1 infection in a model using human peripheral blood mononuclear cell-transplanted NOD/SCID Janus kinase 3 knockout mice. Antimicrob. Agents Chemother. 53, 3887–3893. [PubMed: 19546363]

Higashi-Kuwata N, Ogata-Aoki H, Hattori SI, Hayashi H, Danish M, Aoki M, Shiotsu C, Kawamura T, Ihn H, Kobayashi H, Okada S, Mitsuya H, 2017. Early phase dynamics of traceable mCherry fluorescent protein-carrying HIV-1 infection in human peripheral blood mononuclear cells-transplanted NOD/SCID/Jak3−/− mice. Antivir. Res. 144, 83–92. [PubMed: 28392419]

Honkavuori KS, Shivaprasad HL, Briese T, Street C, Hirschberg DL, Hutchison SK, Lipkin WI, 2011. Novel picornavirus in Turkey poults with hepatitis, California, USA. Emerg. Infect. Dis. 17, 480–487. [PubMed: 21392440]

Koh Y, Nakata H, Maeda K, Ogata H, Bilcer G, Devasamudram T, Kincaid JF, Boross P, Wang YF, Tie Y, Volarath P, Gaddis L, Harrison RW, Weber IT, Ghosh AK, Mitsuya H, 2003. Novel bis-tetrahydrofuranylurethane-containing nonpeptidic protease inhibitor (PI) UIC-94017 (TMC114) with potent activity against multi-PI-resistant human immunodeficiency virus in vitro. Antimicrob. Agents Chemother. 47, 3123–3129. [PubMed: 14506019]

Kovarova M, Swanson MD, Sanchez RI, Baker CE, Steve J, Spagnuolo RA, Howell BJ, Hazuda DJ, Garcia JV, 2016. A long-acting formulation of the integrase inhibitor raltegravir protects

humanized BLT mice from repeated high-dose vaginal HIV challenges. J. Antimicrob. Chemother. 71,1586–1596. [PubMed: 27002074]

Kuper CF, 2006. Histopathology of mucosa-associated lymphoid tissue. Toxicol. Pathol. 34, 609–615. [PubMed: 17067946]

Lee H, Yang SH, Heo D, Son H, Haam S, Suh JS, Yang J, Huh YM, 2016a. Molecular imaging of CD44-overexpressing gastric cancer in mice using T2 MR imaging. J. Nanosci. Nanotechnol. 16, 196–202. [PubMed: 27398445]

Lee HW, Gangadaran P, Kalimuthu S, Ahn BC, 2016b. Advances in molecular imaging strategies for in vivo tracking of immune cells. Biomed. Res. Int. 2016, 1946585. [PubMed: 27725934]

Levesque K, Finzi A, Binette J, Cohen EA, 2004. Role of CD4 receptor down-regulation during HIV-1 infection. Curr. HIV Res. 2, 51–59. [PubMed: 15053340]

Massud I, Martin A, Dinh C, Mitchell J, Jenkins L, Heneine W, Pau CP, Garcia-Lerma JG, 2015. Pharmacokinetic profile of raltegravir, elvitegravir and dolutegravir in plasma and mucosal secretions in rhesus macaques. J. Antimicrob. Chemother. 70, 1473–1481. [PubMed: 25630643]

Nakajima N, Ionescu P, Sato Y, Hashimoto M, Kuroita T, Takahashi H, Yoshikura H, Sata T, 2003. In situ hybridization AT-tailing with catalyzed signal amplification for sensitive and specific in situ detection of human immunodeficiency virus-1 mRNA in formalin-fixed and paraffin-embedded tissues. Am. J. Pathol. 162, 381–389. [PubMed: 12547697]

Nakata H, Amano M, Koh Y, Kodama E, Yang G, Bailey CM, Kohgo S, Hayakawa H, Matsuoka M, Anderson KS, Cheng YC, Mitsuya H, 2007. Activity against human immunodeficiency virus type 1, intracellular metabolism, and effects on human DNA polymerases of 4′-ethynyl-2-fluoro-2′-deoxyadenosine. Antimicrob. Agents Chemother. 51, 2701–2708. [PubMed: 17548498]

Nakata H, Maeda K, Miyakawa T, Shibayama S, Matsuo M, Takaoka Y, Ito M, Koyanagi Y, Mitsuya H, 2005. Potent anti-R5 human immunodeficiency virus type 1 effects of a CCR5 antagonist, AK602/ONO4128/GW873140, in a novel human peripheral blood mononuclear cell nonobese diabetic-SCID, interleukin-2 receptor gamma-chain-knocked-out AIDS mouse model. J. Virol. 79, 2087–2096. [PubMed: 15681411]

Nischang M, Sutmuller R, Gers-Huber G, Audige A, Li D, Rochat MA, Baenziger S, Hofer U, Schlaepfer E, Regenass S, Amssoms K, Stoops B, Van Cauwenberge A, Boden D, Kraus G, Speck RF, 2012. Humanized mice recapitulate key features of HIV-1 infection: a novel concept using long-acting anti-retroviral drugs for treating HIV-1. PLoS One 7, e38853. [PubMed: 22719966]

Okada S, Harada H, Ito T, Saito T, Suzu S, 2008. Early development of human hematopoietic and acquired immune systems in new born NOD/Scid/Jak3null mice intrahepatic engrafted with cord blood-derived CD34 + cells. Int. J. Hematol. 88, 476–482. [PubMed: 19039627]

Rizk ML, Hang Y, Luo WL, Su J, Zhao J, Campbell H, Nguyen BY, Sklar P, Eron JJ Jr., Wenning L, 2012. Pharmacokinetics and pharmacodynamics of once-daily versus twice-daily raltegravir in treatment-naive HIV-infected patients. Antimicrob. Agents Chemother. 56, 3101–3106. [PubMed: 22430964]

Sun Z, Denton PW, Estes JD, Othieno FA, Wei BL, Wege AK, Melkus MW, Padgett-Thomas A, Zupancic M, Haase AT, Garcia JV, 2007. Intrarectal transmission, systemic infection, and CD4+ T cell depletion in humanized mice infected with HIV-1. J. Exp. Med. 204, 705–714. [PubMed: 17389241]

Tilney NL, 1971. Patterns of lymphatic drainage in the adult laboratory rat. J. Anat. 109, 369–383. [PubMed: 5153800]

Tsai CC, Emau P, Follis KE, Beck TW, Benveniste RE, Bischofberger N, Lifson JD, Morton WR, 1998. Effectiveness of postinoculation (R)-9-(2-phosphonylmethoxypropyl) adenine treatment for prevention of persistent simian immunodeficiency virus SIVmne infection depends critically on timing of initiation and duration of treatment. J. Virol. 72, 4265–4273. [PubMed: 9557716]

Van Duyne R, Pedati C, Guendel I, Carpio L, Kehn-Hall K, Saifuddin M, Kashanchi F, 2009. The utilization of humanized mouse models for the study of human retroviral infections. Retrovirology 6, 76. [PubMed: 19674458]

Wade J, Sterjovski J, Gray L, Roche M, Chiavaroli L, Ellett A, Jakobsen MR, Cowley D, Pereira Cda F, Saksena N, Wang B, Purcell DF, Karlsson I, Fenyo EM, Churchill M, Gorry PR, 2010.

Enhanced CD4+ cellular apoptosis by CCR5-restricted HIV-1 envelope glycoprotein variants from patients with progressive HIV-1 infection. Virology 396, 246–255. [PubMed: 19913863]

Yarchoan R, Redfield RR, Broder S, 1986. Mechanisms of B cell activation in patients with acquired immunodeficiency syndrome and related disorders. Contribution of antibody-producing B cells, of Epstein-Barr virus-infected B cells, and of immunoglobulin production induced by human T cell lymphotropic virus, type III/lymphadenopathy-associated virus. J. Clin. Investig. 78, 439–44. [PubMed: 3016028]

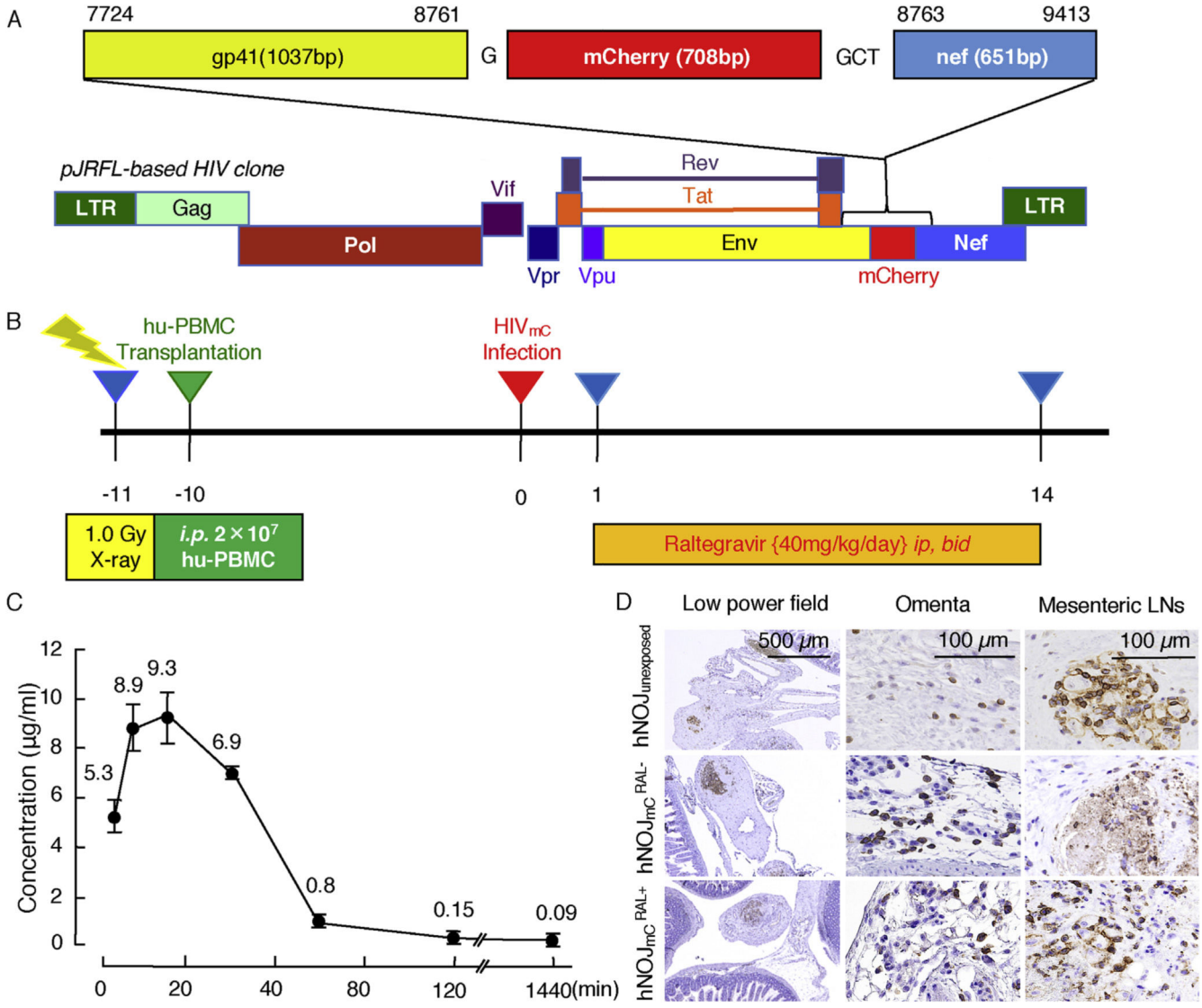

Fig. 1. Construction of pHIV$_{mC}$ and study design.

(A) Genetic map of HIV-1 containing the mC fluorescent protein-encoding gene. HIV-1$_{Jr-Fl}$ was constructed to contain mC fluorescent protein between gp41 and nef proteins. (B) Protocol for radiation, hPBMC transplantation, HIV$_{mC}$ inoculation, RAL treatment and monitoring the dynamics of HIV$_{mC}$ infection. Twenty million hPBMC were transplanted to each mouse 1 day after X-ray exposure. Ten days after the hPBMC transplantation, HIV$_{mC}$ was inoculated *ip.* Twenty-four hours following the HIV$_{mC}$ inoculation, RAL administration (20 mg/kg, twice a day) was implemented and continued over 14 days. Mice were sacrificed on day 14 and subjected to virological, histological, and immunological examinations. (C) Pharmacokinetics of RAL. RAL was administered to each mouse at a dose of 20 mg/kg. Blood samples were taken at 3, 7, 15, 30, 60, 120 and 1440 min and subjected to HPLC analysis (n = 4). The concentration of RAL reached the maximal concentration almost immediately after *ip* administration and subsequently decreased rapidly. The plasma half-life of RAL in this study was approximately 20 min. (D) Re-population of hPBMC in the mesenteric area of each mouse group. Fixed/paraffin-embedded tissue sections were

immunohistologically stained with anti-hCD45 antibody (a pan-lymphocyte marker) and examined under light microscopy. Nuclei were counterstained with Mayer's hematoxylin (blue). Note that $hCD45^{+}$ cells (brown) had been re-populated within the mesenteric lymph nodes comparably among the three mouse groups: $hNOJ_{unexposed}$, $hNOJ_{mC}^{RAL+}$, and $hNOJ_{mC}^{RAL-}$ mice. (For interpretation of the references to colour in this figure legend, the reader is referred to the web version of this article.)

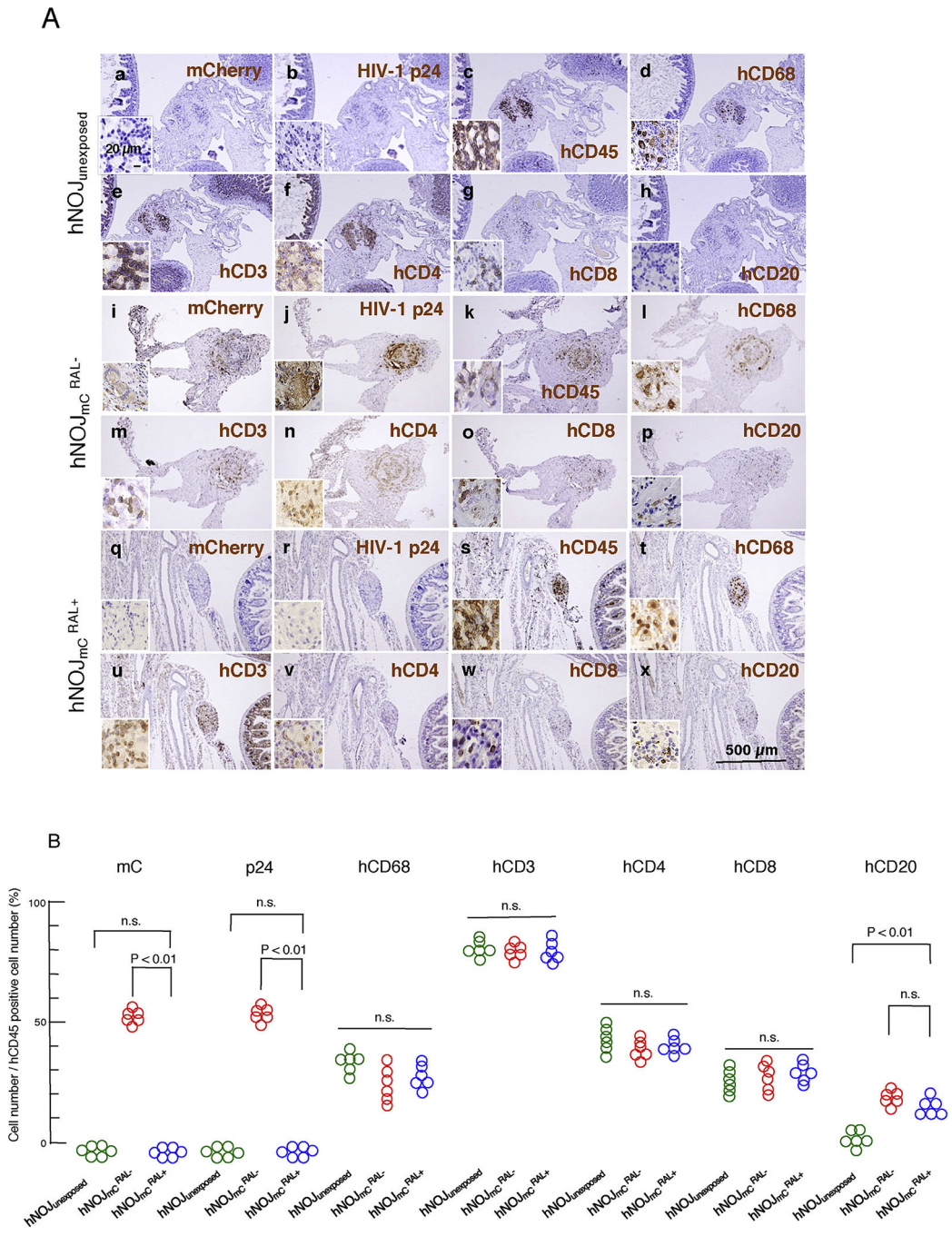

Fig. 2. Representative immunohistochemical staining profiles of mesenteric lymph nodes.

(A) Re-population of human cells in the abdominal cavity. The paraffin sections of mesenteric lymph nodes in each group were immunostained with monoclonal antibodies against mC/DsRed, p24, hCD45, hCD68 (macrophage-specific antigen), hCD3, hCD4, hCD8 and hCD20 (brown). Nuclei were counterstained with Mayer's hematoxylin (blue). Neither mCherry^{+} nor p24^{+} cells were seen in mesenteric (q and r) lymph nodes of $hNOJ_{mC}^{RAL+}$ mice. Cells in mesenteric lymph nodes of $hNOJ_{mC}^{RAL+}$ mice (s–w) showed similar features as seen in $hNOJ_{unexposed}$ mice (c–g). (B) Quantitative analysis of each positive cell

in the mesenteric lymph nodes. Numbers of $mCherry^+$, $p24^+$, $hCD68^+$, $hCD3^+$, $hCD4^+$, $hCD8^+$, and $hCD20^+$ cells per unit area were divided by each corresponding $hCD45^+$ cell number per unit area. No mC^+ or $p24^+$ cells were seen in $hNOJ_{unexposed}$ and $hNOJ_{mC}^{RAL+}$ mice and cell number/$hCD45^+$ cell number was expressed as 0%. Note that the $\%hCD20^+$ was significantly greater in the mesenteric lymph node of $hNOJ_{mC}^{RAL-}$ and $hNOJ_{mC}^{RAL+}$ mice compared to that of $hNOJ_{unexposed}$ mice ($P < 0.01$). No significant differences were observed in $hCD68^+$, $hCD3^+$, $hCD4^+$, or $hCD8^+$ cell numbers among the three mouse groups. (For interpretation of the references to colour in this figure legend, the reader is referred to the web version of this article.)

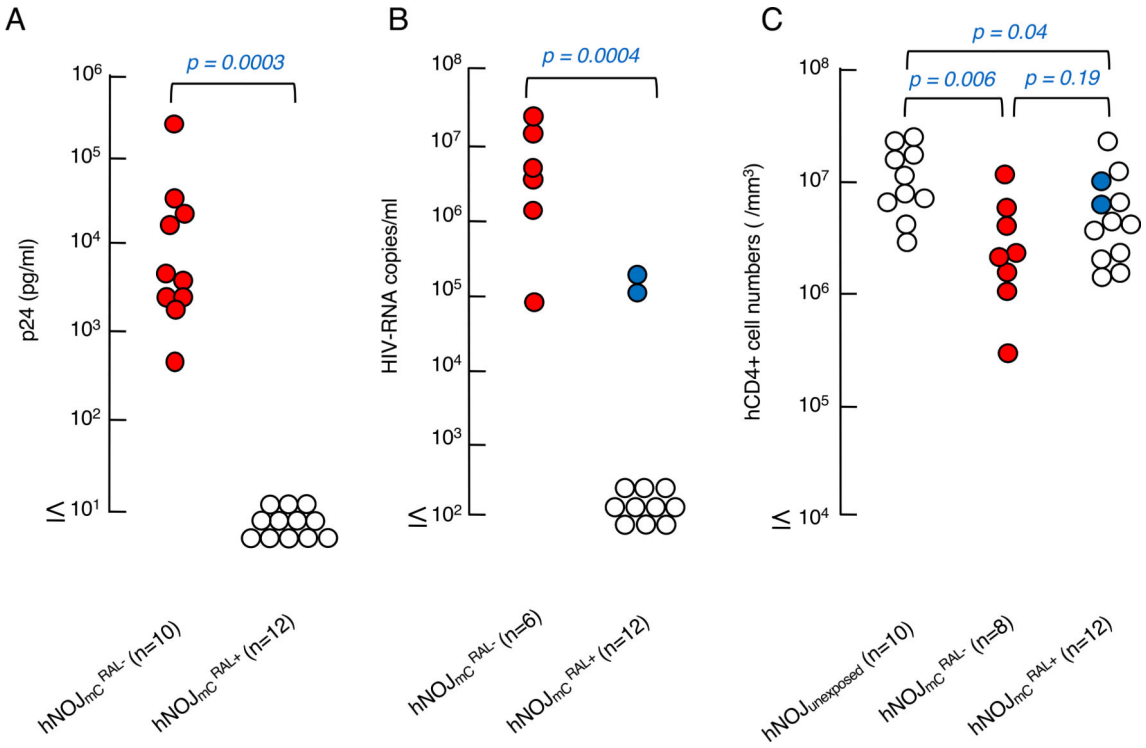

Fig. 3. HIV-1 p24 amounts, pRNA copies and hCD4$^+$ cell counts in each hNOJ mouse group with or without RAL treatment.

(A) Amounts of plasma p24 antigen. Plasma from the hNOJ$_{mC}^{RAL-}$ and hNOJ$_{mC}^{RAL+}$ mice were examined using a fully automated chemiluminescent enzyme immunoassay on day 14 after HIV$_{mc}$ inoculation. Note that the amounts of p24 in plasma were high in hNOJ$_{mC}^{RAL-}$ mice while RAL significantly suppressed the plasma p24 antigen as examined on day 14 after HIV$_{mc}$ inoculation. (p = 0.0003 compared to hNOJ$_{mC}^{RAL+}$ mice). (B) Amounts of pRNA copies. Blood samples were collected on day 14 and subjected to the determination of pRNA copy numbers. Note that the copy numbers in hNOJ$_{mC}^{RAL-}$ mice were high on day 14. (P = 0.0004 compared to hNOJ$_{mC}^{RAL+}$ mice). (C) Numbers of CD4$^+$ cells in each mouse group. hPBMc recovered on day 14 after HIV$_{mc}$ inoculation were counted and subjected to flow cytometry.

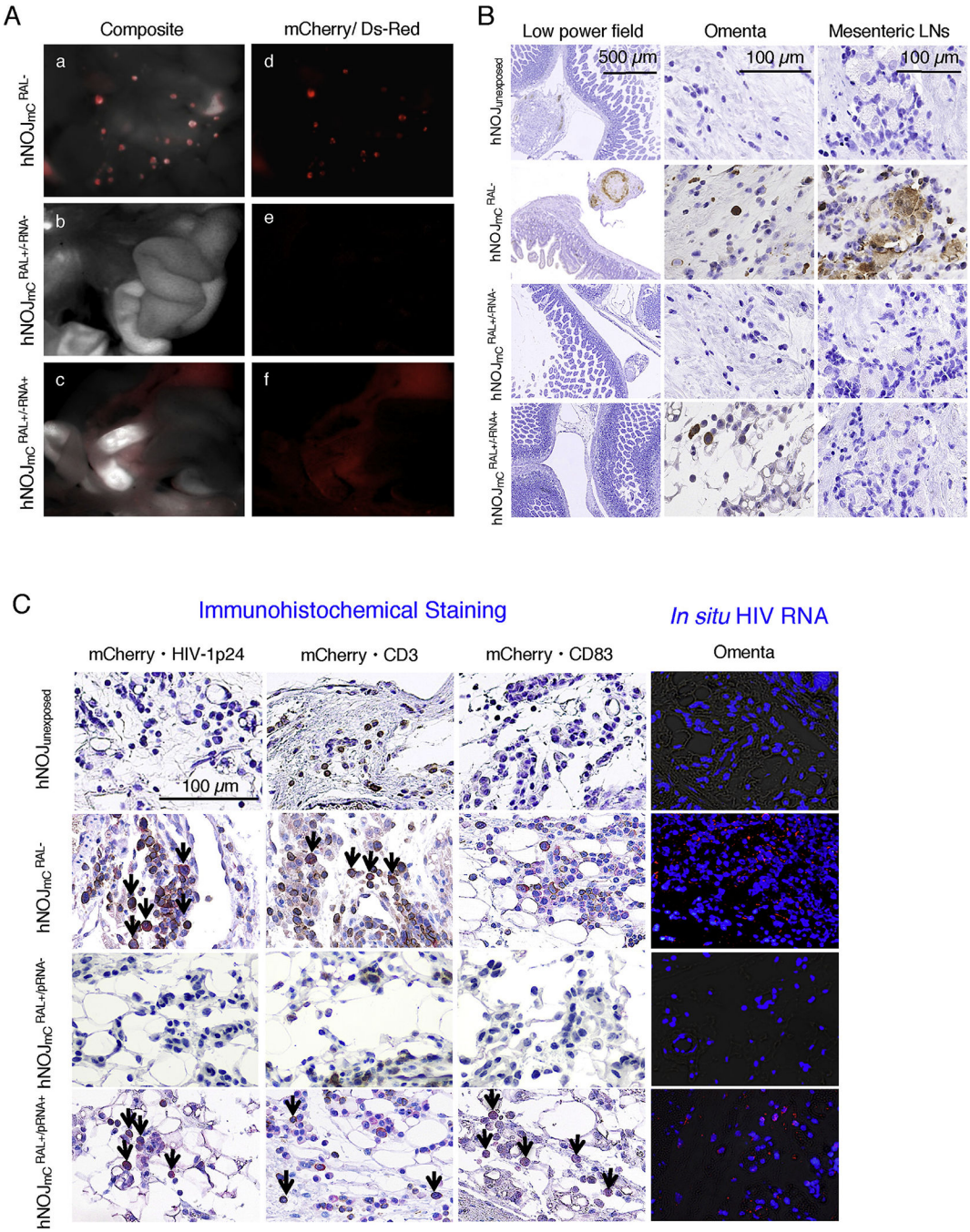

Fig. 4. Prevention of HIV_{mC} infection with RAL treatment in hNOJ mice.

(A) Representative *in vivo* images. No mC signals were seen in abdominal area in all of $hNOJ_{mC}^{RAL+}$ mice, except two $hNOJ_{mC}^{RAL+/pRNA+}$ mice. Composite images (a–c) consisting of autoflurescence spectra and mC specific spectra demonstrate the location of mC positive organs. By day 14 after HIV_{mC} inoculation, mC signal was mainly detected in mesenteric lymph nodes and the omentum of $hNOJ_{mC}^{RAL-}$ mice (a and d). The mC signals were hardly recognized in $hNOJ_{mC}^{RAL+}$ mice with undetectable pRNA levels (b and e). $hNOJ_{mC}^{RAL+}$ mice

with detectable pRNA copies showed diffuse mC signals in their omentum (c and f). In panels a and d of Figure 4-A, the multiple spotty red signals are mC^+ mesenteric lymph nodes, whereas the dimly red areas are mC^+ omenta. In panels c and f of Figure 4-A, although significant mC signals are seen in omenta, no mC^+ lymph nodes are seen. (B) Representative p24 profiles among mouse groups. No p24 positive cells were observed in the abdominal area in all the $hNOJ_{mC}^{RAL+}$ mice, except two $hNOJ_{mC}^{RAL+/pRNA+}$ mice. The $p24^+$ cells were observed in the omenta of those two $hNOJ_{mC}^{RAL+/pRNA+}$ mice as well as all $hNOJ_{mC}^{RAL-}$ mice. No $p24^+$ cells were observed in the mesenteric lymph node of $hNOJ_{mC}^{RAL+/pRNA+}$ mice, whereas a number of p24 positive cells were found in $hNOJ_{mC}^{RAL-}$ mice. (C) Representative double-staining profiles and *in situ* hybridization data. HIV-RNA was not detected in the mesenteric lymph nodes of $hNOJ_{mC}^{RAL+/pRNA-}$, while no HIV-RNA was observed in $hNOJ_{unexposed}$ (very right columns). HIV-RNA was detected in the omenta of $hNOJ_{mC}^{RAL+/pRNA+}$, however, the number of such HIV-RNA^+ cells was much smaller than in the $hNOJ_{mC}^{RAL-}$. Nuclei were stained with DAPI. Arrows denote mC^+ plus $p24^+$ cells, mC^+ plus $hCD3^+$ cells, and mC^+ plus $hCD83^+$ cells. Nuclei were stained with hematoxylin and seen in blue. mC + cells are stained in red, whereas HIV-1 $p24^+$, $CD3^+$, and $CD83^+$ cells are stained in brown. (For interpretation of the references to colour in this figure legend, the reader is referred to the web version of this article.)

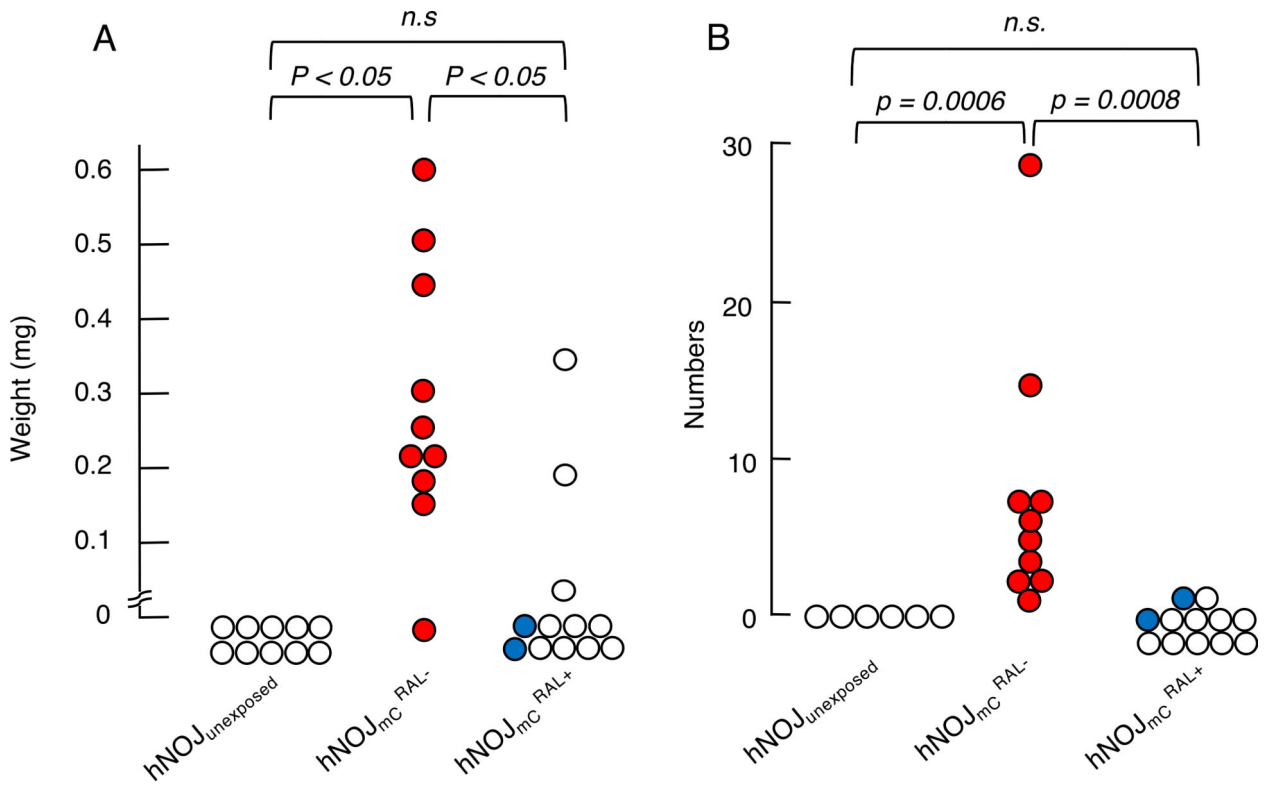

Fig. 5. Comparison of the weights and numbers of mesenteric lymph nodes among three hNOJ mouse groups with or without RAL treatment.

For comparison, the largest lymph node in each mouse was examined. The largest lymph nodes in each mouse less than 0.01 mg were expressed as 0 mg in Panel A. For comparison of the numbers of lymph nodes, mC signal-emitting lymph nodes were counted using the Maestro™ system as shown in Panel B. Statistical analyses were performed using a nonparametric multiple comparison called Bonferroni method.

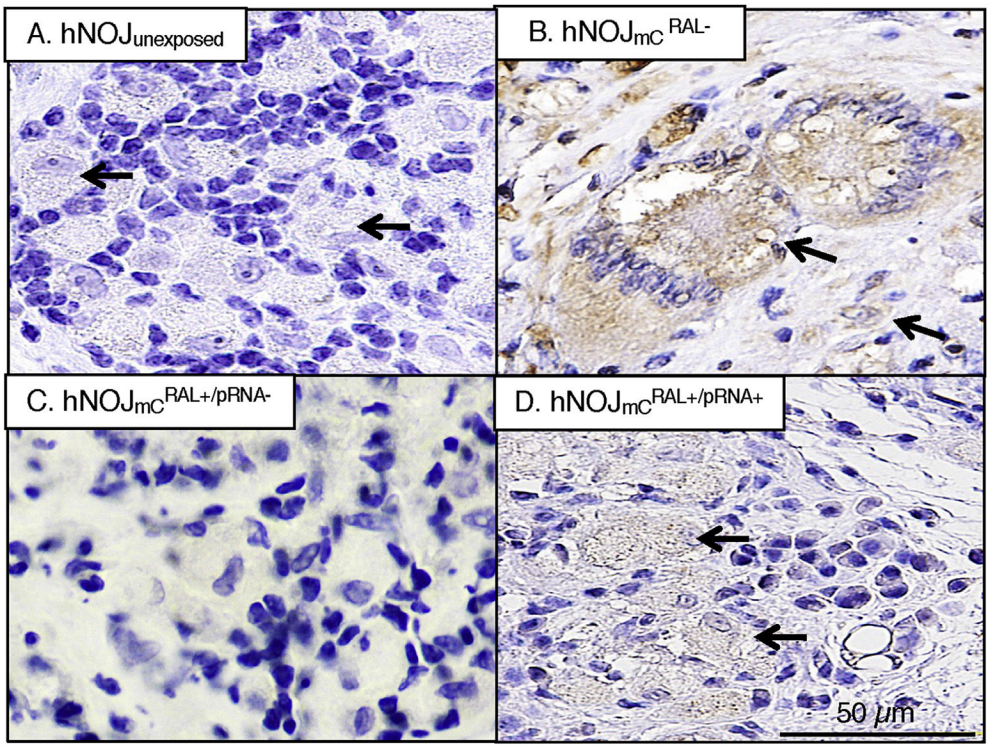

Fig. 6. Morphologic profiles of mesenteric lymph nodes.

A number of multinuclear giant cells and cytolysis were seen in HIV_{mC}^{RAL-} mice. Only cytolysis was seen in one of the two $hNOJ_{mC}^{RAL+/pRNA+}$ mice. Neither was seen in the other $hNOJ_{mC}^{RAL+/pRNA+}$ mouse, $hNOJ_{unexposed}$ mice, or $hNOJ_{mC}^{RAL+/pRNA-}$ mice.